


Article

# High-Throughput Small-Molecule Crystallography at the ‘Belok’ Beamline of the Kurchatov Synchrotron Radiation Source: Transition Metal Complexes with Azomethine Ligands as a Case Study

Vladimir A. Lazarenko <sup>1</sup> , Pavel V. Dorovatovskii <sup>1</sup>, Yan V. Zubavichus <sup>1</sup>, Anatolii S. Burlov <sup>2</sup> ,  
Yurii V. Koshchienko <sup>2</sup> , Valery G. Vlasenko <sup>3</sup>  and Victor N. Khrustalev <sup>4,\*</sup> 

<sup>1</sup> National Research Center “Kurchatov Institute”, Moscow 123182, Russian Federation; vladimir.a.lazarenko@gmail.com (V.A.L.); paulgemini@mail.ru (P.V.D.); yzubav@gmail.com (Y.V.Z.)

<sup>2</sup> Institute of Physical and Organic Chemistry of Southern Federal University, Rostov-on-Don 344090, Russian Federation; asburlov@ipoc.sfedu.ru (A.S.B.); yukoshch@ipoc.sfedu.ru (Y.V.K.)

<sup>3</sup> Institute of Physics of Southern Federal University, Rostov-on-Don 344090, Russian Federation; v\_vlasenko@rambler.ru

<sup>4</sup> Peoples’ Friendship University of Russia (RUDN University), Moscow 117198, Russian Federation

\* Correspondence: vnkhrustalev@gmail.com

Academic Editor: William Clegg

Received: 10 October 2017; Accepted: 24 October 2017; Published: 28 October 2017

**Abstract:** This paper concisely describes capabilities of the ‘Belok’ beamline at the Kurchatov synchrotron radiation source, related to high-throughput small-molecule X-ray crystallography. As case examples, a series of four novel transition metal complexes with azomethine ligands were selected. The complexes demonstrate somewhat unexpected changes in the coordination geometry and nuclearity in response to the introduction of substituents in the ligand’s periphery.

**Keywords:** Kurchatov synchrotron radiation source; transition metals; azomethine ligands; secondary interactions; crystal structure

## 1. Introduction

The use of synchrotron radiation in small-molecule crystallography has probably not provided such impressive breakthroughs as has the field of macromolecular crystallography [1], but still it remains a heavily demanded and rapidly emerging field of research [2–5]. Recently commissioned beamlines dominantly or partly dedicated to small-molecule crystallography include, among others, I19 at the Diamond Light Source [6,7], MX1 at the Australian Synchrotron [8], and BL2D-SMC at the Pohang Light Source [9]. Examples of approved and very productive dedicated instruments include beamlines 11-3-1 [10] and 12-2-2 [11] at the Advanced Light Source (Berkeley, CA, USA). The use of synchrotron radiation provides some evident advantages, such as the possibility of studying tiny and imperfect crystals, reducing mean data acquisition time, collecting diffraction data to high 2θ scattering angles to improve the quality of electron density distribution maps, etc. Real-time crystallographic studies of dynamical processes in crystals, such as solid-state reactions, phase transitions, conformational changes upon photoexcitation, become increasingly important [12–15].

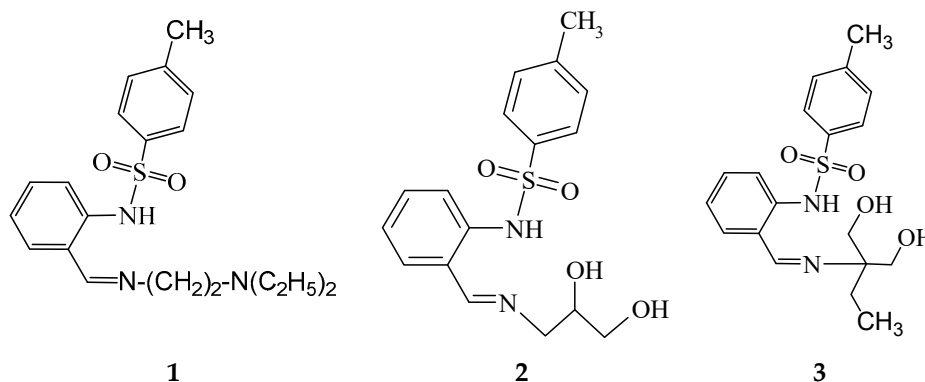
Complexes of transition metals with azomethines (also referred to as Schiff bases) are the focus of contemporary research due to a number of physicochemical properties making them attractive for applications. There are numerous examples of their photoactivity (photo- or electroluminescence) enabling their use as functional layers in thin-filmed OLEDs [16–18].

Transition metal complexes with  $ML_4$ ,  $ML_5$ , and  $ML_6$  coordination cores (where L is an N/O/S ligand) are of fundamental importance for structural biology as synthetic models of metalloproteins. Structural information on model complexes can be used for the interpretation, verification, and restrained fitting of experimental electron density maps of real metalloproteins derived from limited-resolution experimental diffraction data [19–21].

Organic ligands bearing one or several sulfonamide moieties very often induce biological activity in their derivatives [22,23]. For a series of iron-based complexes, the spin crossover effect was reported [24,25]. Polynuclear transition metal complexes with azomethines are also promising as single-molecule magnets or at least as synthetically affordable models to study exchange interactions between paramagnetic sites and to verify modern theoretical approaches to the prediction of magnetic properties [26–32].

The deliberate introduction of alcoholic groups into the peripheral part of azomethine ligands is a convenient route to polynuclear complexes since a hydroxy group is a versatile O-donor prone to the formation of multi-center bridging bonds. Nevertheless, modern knowledge of regularities underlying the structure formation of transition metal complexes with polydentate chelate ligands is still insufficient to enable the genuinely rational design of polynuclear complexes of required stoichiometry, nuclearity and spatial geometry.

In the present paper, we report crystal structures of a series of novel transition metal complexes of 2-*N*-tosylaminobenzaldehyde azomethines bearing aliphatic amino- and alcoholic groups in the ligand's periphery 1-3, as shown in Scheme 1. More specifically, complexes **1-Fe**, **2-Zn**, **3-Cu** and **3-Ni** were synthesized from the respective free ligands and metal salts to be studied by single-crystal X-ray diffraction at a synchrotron source. To the best of our knowledge (based on an *ad hoc* CSD search), no crystal structures of metal complexes derived from 2-*N*-tosylaminobenzaldehyde azomethines with only C,N,O acyclic substituents have yet been reported. Despite the presence of a coordinately active core common for all three ligands, identical oxidation states +2 and similar ionic radii of the 3d-metals, the resultant complexes demonstrated different nuclearity, viz. **1-Fe** and **2-Zn** are monomers, **3-Cu** is a dimer, and **3-Ni** is a supramolecular assembly of tetranuclear clusters.



**Scheme 1.** Chemical diagrams of azomethine ligands with amine and alcoholic substituents used for the synthesis of complexes.

## 2. Materials and Methods

### 2.1. General Description of the 'Belok' Beamline at the Kurchatov Synchrotron Radiation Source

The Kurchatov synchrotron radiation source located in Moscow, Russia, and operated by the National Research Centre, the "Kurchatov Institute", is a dedicated 2nd generation source based on an electron storage ring Siberia-2 (circumference 124 m, electron energy 2.5 GeV, mean current 70–100 mA). It was put into operation in early 2000 s. The total number of beamlines open to user services is 13 and several large-scale instrumentation upgrade programs are currently underway. The 'Belok' beamline

is one of the 1st priority beamlines, commissioned in 2004 [33]. It relies on a bending magnet as a radiation source. Its optical scheme includes the following major components:

- a Si double-crystal monochromator in the (1,−1) configuration providing a fixed-exit beam position. The second crystal is sagittally bent to focus the beam in the horizontal plane with the focal spot coinciding with the 2D position-sensitive detector;
- a multi-segment total reflection mirror providing focusing in the vertical plane and higher harmonics suppression;
- a diffractometer.

A more detailed description of the beamline hardware can be found elsewhere [33]. The diffractometer itself is composed of the following components:

- a Rayonix SX-165 position-sensitive CCD detector with a dynamic range of 16 bits;
- a MARdtb single-axis goniometer. The goniometer provides a high-precision  $\varphi$ -scanning; the sample-to-detector distance can be automatically selected over a range 43–380 mm and the detector plane can be tilted up to  $29.5^\circ$  to extend the  $2\theta$  scattering angle range.
- LN<sub>2</sub> low-temperature device by Oxford Cryosystems.

A general view of the diffractometer at the ‘Belok’ beamline is shown in Figure 1. Single crystals under study are mounted using cryoloops of different sizes. The wavelength range is 2.5–0.5 Å, most frequently a value around 1 Å is selected. At a wavelength of 0.97 Å, a sample-to-detector distance of 43 mm, and detector plane tilt of  $15^\circ$ , the experimental geometry provides apparent resolution of  $d_{\min} = 0.78$  Å,  $(\sin\theta/\lambda)_{\max} = 0.65$  Å<sup>−1</sup>. To ensure sufficient completeness of a diffraction dataset, at least two runs with different orientations of the single-crystal being measured are needed, which implies thawing, remounting on a cryoloop, and refreezing of the crystal. It is also often practical to perform a few independent runs with different exposure times to improve on the accuracy of intensity measurements of weak high-angle reflections.

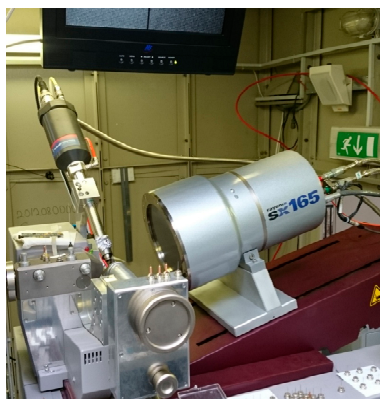


**Figure 1.** General view of the diffractometer unit at the ‘Belok’ beamline.

An assortment of freely distributed software suites are in routine use at the beamline, such as XDS [34], iMOSFLM [35] and other routines from the CCP4 package [36], and DIASL [37] (processing of raw frames, including peak search, indexing, unit cell parameters refinement, and peak intensity integration). Pointless and Scala are used for space group determination and intensity scaling [38]. Crystal structures are solved and refined with a very user-friendly GUI of Olex2 [39] that is based on original algorithms by G.M. Sheldrick [40–42].

The beamline was originally designed for the needs of macromolecular crystallography. Due to the actual structure of demand from the Russian users’ community, the available beamtime is now shared between MX, small-molecule crystallography, powder diffraction, and polymer scattering

applications. Examples of protein structures solved and refined against experimental diffraction data collected at the 'Belok' beamline include: uridine phosphorylase, laccases, ribonuclease, etc. [43–47]. In the powder diffraction mode, the emphasis is placed on real-time studies on new phase emergence and phase transitions for functionally sound materials [48,49]. For X-ray scattering experiments on partly crystalline materials, we try to fully exploit the 2D nature of X-ray images to get insight into changes of preferred orientation and crystallinity of polymers, liquid crystals, etc. [50,51].

In the small-molecule crystallography mode, the typical size of a crystal ranges from 100 to 300  $\mu\text{m}$ , although successful measurements for crystals on the order of 10  $\mu\text{m}$  in at least one dimension have been documented. The minimum exposure time is 0.8 s per frame as defined by the  $\varphi$ -scan drive. Overall, the capabilities of the beamline do not exceed those of the most advanced 3rd generation synchrotron sources. Nevertheless, the apparent advantages of such a moderate-level synchrotron-based diffractometer over serial in-lab devices look attractive to numerous user groups. And the number of loyal users of the 'Belok' beamline has expanded explosively over the last few years since the start of operation in this mode.

The molecular structure of a crystal under study can be visualized after a couple of minutes of data collection (based on 30–40 diffraction frames), which enables a high-throughput screening of extended series of similar species in a hunt for a specific target molecular geometry. The mean productivity of the beamline in the small-molecule crystallography mode is 25–30 new crystal structures per week and roughly 500 per year. Examples of recently published challenging crystal structures include cage polynuclear metal-containing organosiloxanolates [52–54], synthetic analogs of naturally occurring alkaloids [55] and other biologically active substances [56], unstable catalysis-related intermediates [57,58], products of photoinitiated single crystal-single crystal solid-state reactions [59], etc.

## 2.2. Synthesis of Free Ligands and Their Derived Metal Complexes

Reactants and organic solvents used in the synthesis of free ligands, viz. 2-amino-2-ethyl-1,3-propanol, 3-amino-1,2-propanediol, triethylamine, L(+)-ascorbic acid, *N,N*-diethylethylenediamine,  $\text{Fe}(\text{BF}_4)_2 \cdot 6\text{H}_2\text{O}$ ,  $\text{Zn}(\text{CH}_3\text{COO})_2 \cdot 2\text{H}_2\text{O}$ ,  $\text{Cu}(\text{CH}_3\text{COO})_2 \cdot \text{H}_2\text{O}$ ,  $\text{Ni}(\text{CH}_3\text{COO})_2 \cdot 4\text{H}_2\text{O}$ , and acetonitrile were purchased from Alfa Aesar (Ward Hill, MA, USA) and used without further purification. 2-(*N*-tosylamino)benzaldehyde was synthesized using the protocol as reported elsewhere [60].

### *N*-[2-(2-diethylaminoethyliminomethyl)phenyl]-4-methylbenzenesulfonamide (**1**)

A solution of *N,N*-diethylethylenediamine (0.58 g, 5 mmol) in benzene (20 mL) was added to a solution of 2-(*N*-tosylamino)benzaldehyde (1.38 g, 5 mmol) in benzene (20 mL). The reaction mixture was boiled in a flask with a Dean-Stark head for 2 h until complete removal of water. Then the volume of the reaction mixture was reduced to 15 mL using a rotary evaporator. A precipitate formed upon cooling. Yield is 1.59 g (80%). Light brown powder, m.p. 44–45 °C. Calcd. for  $\text{C}_{20}\text{H}_{27}\text{N}_3\text{O}_2\text{S}$ : C 64.31, H 7.29, N 11.25%. Found, %: C 64.28, H 7.32, N 11.20%. IR (in the solid phase),  $\nu$ ,  $\text{cm}^{-1}$ : 1600 s (CH=N), 1340 s ( $\nu_{\text{as}}\text{SO}_2$ ), 1164 vs ( $\nu_{\text{s}}\text{SO}_2$ ).  $^1\text{H}$  NMR (in  $\text{DMSO}-d_6$ ),  $\delta$ , ppm: 0.94 (6H, t,  $^3J = 7.2$  Hz, 2  $\text{CH}_2\text{CH}_3$ ), 2.29 (3H, s, C- $\text{CH}_3$ ), 2.53 (4H, q,  $^3J = 7.2$  Hz, 2  $\text{CH}_2\text{CH}_3$ ), 2.71 (2H, t,  $^3J = 6.3$  Hz,  $\text{CH}_2\text{CH}_2\text{N}(\text{C}_2\text{H}_5)_2$ ), 3.68 (2H, t,  $^3J = 6.3$  Hz,  $\text{CH}_2\text{CH}_2\text{N}(\text{C}_2\text{H}_5)_2$ ), 7.04 (1H, t,  $^3J = 7.5$  Hz,  $\text{CH}_a$ ), 7.30 (2H, d,  $^3J = 8.1$  Hz,  $\text{C}_{\text{Ar}}\text{-H}$ ), 7.34 (1H, d,  $^3J = 7.5$  Hz,  $\text{C}_{\text{Ar}}\text{-H}$ ), 7.45 (2H, t,  $^3J = 6.3$  Hz,  $\text{C}_{\text{Ar}}\text{-H}$ ), 7.67 (2H, d,  $^3J = 8.1$  Hz,  $\text{C}_{\text{Ar}}\text{-H}$ ), 8.45 (1H, s, CH=N).

### Bis-[2-(2-diethylaminoethyliminomethyl)phenyl]-4-methylbenzenesulfonamidato}iron(II) (**1-Fe**)

A solution of  $\text{Fe}(\text{BF}_4)_2 \cdot 6\text{H}_2\text{O}$  (0.168 g, 0.5 mmol) in methanol also containing L-ascorbic acid (0.088 g, 0.5 mmol) was mixed with a solution of free ligand **1** (0.37 g, 1 mmol) in methanol (20 mL). To adjust pH of the reaction mixture, a solution of triethylamine (0.1 g, 1 mmol) in methanol (10 mL) was added. The mixture was stirred for 1 h at room temperature. Brick red precipitate formed was filtered off and recrystallized from methanol. All synthesis steps were performed in an argon atmosphere using the Schlenk technique. Yield is 60%. M.p. > 260 °C. Calcd. for  $\text{C}_{40}\text{H}_{52}\text{N}_6\text{O}_4\text{S}_2\text{Fe}$ : C

59.99, H 6.54, N 10.49, Fe 6.97%. Found, %: C 60.10, H 6.48, N 10.55, Fe 7.02%. IR (in nujol),  $\nu$ ,  $\text{cm}^{-1}$ : 1608 (CH=N), 1299 ( $\nu_{\text{as}}\text{SO}_2$ ), 1127 ( $\nu_{\text{s}}\text{SO}_2$ ).

#### N-[2-[(E)-2,3-dihydroxypropyliminomethyl]phenyl]-4-methylbenzenesulfonamide (**2**)

A solution of 3-amino-1,2-propandiol in 1:1 toluene-ethanol mixture (5 + 5 mL) was added to a solution of 2-N-tosylaminobenzaldehyde (2.75 g, 10 mmol) in toluene (20 mL). The mixture was refluxed for 3 h. The volume of the reaction mixture was reduced to 15 mL using a rotary evaporator. A precipitate formed upon cooling. The precipitate was filtered off, washed with toluene, dried, and recrystallized from ethanol. Pale yellow powder. Yield is 3.25 g (94%). M.p. 149–150 °C. Calcd. for  $\text{C}_{17}\text{H}_{20}\text{N}_2\text{O}_4\text{S}$ : C, 58.60; H, 5.79; N, 8.04. Found: C, 58.54; H, 5.85; N, 8.19. IR,  $\nu$ ,  $\text{cm}^{-1}$ : 3219 broad m (OH, NH), 1633 s (CH=N), 1335 s ( $\nu_{\text{as}}\text{SO}_2$ ), 1158 vs ( $\nu_{\text{as}}\text{SO}_2$ ).  $^1\text{H}$  NMR (in  $\text{DMSO-d}_6$ ),  $\delta$ , ppm: 2.35 (3H, s,  $\text{CH}_3$ ), 3.47–3.54 (3H, m,  $\text{CH}_2$ , CH), 3.84 (2H, q,  $^3\text{J} = 7.2$  Hz,  $\text{CH}_2$ ), 4.50 (1H, s, OH), 4.68 (1H, s, OH), 7.02 (1H, t,  $^3\text{J} = 7.5$  Hz,  $\text{C}_{\text{Ar}}\text{-H}$ ), 7.27 (3H, t,  $^3\text{J} = 8.4$  Hz,  $\text{C}_{\text{Ar}}\text{-H}$ ), 7.39 (1H, d,  $^3\text{J} = 7.8$  Hz,  $\text{C}_{\text{Ar}}\text{-H}$ ), 7.49 (1H, d,  $^3\text{J} = 8.4$  Hz,  $\text{C}_{\text{Ar}}\text{-H}$ ), 7.68 (2H, d,  $^3\text{J} = 8.1$  Hz,  $\text{C}_{\text{Ar}}\text{-H}$ ), 8.36 (1H, s, CH=N), 13.23 (1H, s, NH).

#### Bis{N-[2-[(E)-2,3-dihydroxypropyliminomethyl]phenyl]-4-methylbenzenesulfonamidato} zinc(II), DMF solvate (**2-Zn**)

A hot solution of zinc acetate dihydrate (0.275 g, 0.75 mmol) in 1:1 ethanol-acetonitrile mixture (3 + 3 mL) was added to a hot solution of the free ligand **2** (0.553 g, 1.5 mmol) in acetonitrile (5 mL). The reaction mixture was refluxed for 2 h. A precipitate formed upon cooling. The precipitate was filtered off, washed with acetonitrile and recrystallized from 25:2 acetonitrile-DMF mixture. Colorless crystals. Yield is 0.403 g (65%). M.p. > 260 °C. Calcd. for  $\text{C}_{35.5}\text{H}_{41.5}\text{N}_{4.5}\text{O}_{8.5}\text{S}_2\text{Zn}$ : C, 55.73; H, 5.64; N, 8.79; Zn, 8.21. Found: C, 53.27; H, 5.49; N, 8.49; Zn, 7.91 (the experimental chemical composition better corresponds to DMF monosolvate rather than hemisolvate as determined crystallographically, which probably indicates a slow solvent loss during storage of the crystals under ambient conditions). IR,  $\nu$ ,  $\text{cm}^{-1}$ : 3367 broad m (OH), 1631 vs (CH=N), 1287 vs ( $\nu_{\text{as}}\text{SO}_2$ ), 1133 vs ( $\nu_{\text{as}}\text{SO}_2$ ).  $^1\text{H}$  NMR (in  $\text{DMSO-d}_6$ ),  $\delta$ , ppm: 2.25 (6H, s,  $\text{CH}_3$ ), 2.72 and 2.88 (3H, s,  $(\text{CH}_3)_2\text{NCHO}$  of DMF), 3.10–3.26 (4H, m,  $\text{CH}_2$ ), 3.46–3.95 (4H, m,  $\text{CH}_2$ ), 4.27–4.36 (2H, m, CH), 4.58 (2H, d,  $^3\text{J} = 5.1$  Hz, OH), 5.05 (2H, d,  $^3\text{J} = 8.7$  Hz, OH), 6.86 (2H, t,  $^3\text{J} = 7.2$  Hz,  $\text{C}_{\text{Ar}}\text{-H}$ ), 7.16–7.36 (8H, m,  $\text{C}_{\text{Ar}}\text{-H}$ ), 7.49 (2H, d,  $^3\text{J} = 7.8$  Hz,  $\text{C}_{\text{Ar}}\text{-H}$ ), 7.91 (2H, d,  $^3\text{J} = 8.1$  Hz,  $\text{C}_{\text{Ar}}\text{-H}$ ), 7.96 (2H, d,  $^3\text{J} = 8.1$  Hz,  $\text{C}_{\text{Ar}}\text{-H}$ ), 8.45 (2H, s, CH=N).

#### Bis{N-[2-[(E)-2,2-bis(hydroxymethyl)butyliminomethyl]phenyl]-4-methylbenzenesulfonamide} dicopper(II) (**3-Cu**)

The synthesis of a **3-Cu** complex was performed in situ without a dedicated stage of free ligand isolation. A solution of 2-amino-2-ethyl-1,3-propandiol 0.12 g (1 mmol) in methanol was added to a solution of 2-N-tosylaminobenzaldehyde (0.28 g, 1 mmol) in methanol (20 mL). The mixture was boiled for 2 h then a solution of copper acetate monohydrate (0.2 g, 1 mmol) in methanol (20 mL) was added. The reaction mixture was boiled again for 1 h and a green precipitate formed upon cooling. The precipitate was filtered off, washed with hot ethanol and dried in vacuo at 100 °C. Green powder yield is 65%. M.p. > 250 °C. Calcd. for  $\text{C}_{38}\text{H}_{44}\text{N}_4\text{O}_8\text{S}_2\text{Cu}_2$ : C 52.10, H 5.06, N 6.40, Cu 14.51%. Found: C 52.17, H 5.18, N 6.52, Cu 14.21%. IR (in nujol),  $\nu$ ,  $\text{cm}^{-1}$ : 3500 broad (OH), 1637 vs (CH=N), 1281 vs ( $\nu_{\text{as}}\text{SO}_2$ ), 1133 vs ( $\nu_{\text{s}}\text{SO}_2$ ).

#### Tris{ $\mu_4$ -[2-[(E)-2,2-bis(hydroxymethyl)butyliminomethyl]phenyl]-4-methylbenzenesulfonamide- $\kappa\text{N,N}'$ , $\kappa^3\text{O}$ ]ethanolato)-( $\mu_3$ -oxo)-tris(aqua)-tetra-nickel, adduct with KOAc, ( $\text{HNEt}_3$ )OAc, acetic acid solvate (**3-Ni**)

The synthesis of **3-Ni** complex was performed in situ without a dedicated stage of free ligand isolation. A solution of 2-amino-2-ethyl-1,3-propandiol (0.12 g, 1 mmol) in ethanol was added to a solution of 2-N-tosylaminobenzaldehyde (0.28 g, 1 mmol) in ethanol (20 mL). The reaction mixture was boiled for 2 h then a solution of nickel acetate tetrahydrate (0.248 g, 1 mmol) in ethanol (5 mL)

also containing triethylamine (0.1 g, 1 mmol) was added and the mixture was boiled again for 1 h. Since no precipitate formed spontaneously upon cooling to room temperature, the reaction mixture was additionally basified by adding a solution of KOH (0.11 g, 2 mmol) in ethanol (5 mL). Green precipitate formed was filtered off and dried in vacuo at 100 °C. Green crystals. Yield is 60%. M.p. > 260 °C. Since the actual stoichiometry and structure of the complex as established by single-crystal X-ray diffraction (see below) appeared totally different from expectations, no chemical analysis was performed. IR (in nujol),  $\nu$ ,  $\text{cm}^{-1}$ : 1679 vs (CH=N), 1297 vs ( $\nu_{\text{as}}\text{SO}_2$ ), 1130 vs ( $\nu_{\text{s}}\text{SO}_2$ ).

### 2.3. Chemical and Spectroscopic Characterization

C, H, N, elemental analyses were carried out with a TCM 480 apparatus (Carlo Erba Instrument, Milan, Italy) using sulfanilamide as a reference. The metal content was determined gravimetrically in the analytical laboratory of the Institute of Physical and Organic Chemistry (SFU, Rostov-on-Don, Russia). Melting points were measured on a Kofler hot bench (Wagner & Munz GmbH, Munich, Germany). Infrared spectra (4000–400  $\text{cm}^{-1}$ ) were recorded on an Excalibur-3100 FT-IR spectrophotometer (Varian Inc., Palo Alto, CA, USA) for powders suspended in nujol in the total external reflection mode.  $^1\text{H}$  NMR spectra were measured on an Unity 300 spectrometer (Varian Inc., Palo Alto, CA, USA) at ambient temperature in DMSO- $d_6$  using the signal of residual 2H of the solvent as an internal reference.

### 2.4. Crystal Structure Determinations

X-ray diffraction data were collected at the ‘Belok’ beamline ( $\lambda = 0.96990 \text{ \AA}$ ) of the Kurchatov Synchrotron Radiation Source. All datasets were collected at 100 K. In total, 480–720 frames were collected with an oscillation range of  $1.0^\circ$  in the  $\phi$  scanning mode using two different orientations for each crystal. The semiempirical correction for absorption was applied using the Scala program [38].

The data were indexed and integrated using the utility iMOSFLM from the CCP4 software suite [35,36]. For details, see Table 1. The structures were solved by intrinsic phasing modification of direct methods [42] and refined by a full-matrix least-squares technique on  $F^2$  with anisotropic displacement parameters for all non-hydrogen atoms and hydrogen atoms involved in H-bonding. H-bonding-silent hydrogen atoms were placed in calculated positions and refined within the riding model with fixed isotropic displacement parameters. All calculations were carried out using the SHELXTL program [40,41].

**Table 1.** General crystallographic information on complexes studied.

Compound	1-Fe	2-Zn	3-Cu	3-Ni
Empirical formula	$\text{C}_{40}\text{H}_{52}\text{FeN}_6\text{O}_4\text{S}_2$	$\text{C}_{35.5}\text{H}_{41.5}\text{N}_{4.5}\text{O}_{8.5}\text{S}_2\text{Zn}$	$\text{C}_{38}\text{H}_{44}\text{Cu}_2\text{N}_4\text{O}_8\text{S}_2$	$\text{C}_{718}\text{H}_{931}\text{K}_4\text{N}_{73}\text{Ni}_{48}\text{O}_{220}\text{S}_{36}$
$f_w$	800.84	796.72	875.97	18232.06
$T$ , K	100 (2)	100 (2)	100 (2)	100 (2)
Crystal size, mm	$0.20 \times 0.15 \times 0.02$	$0.20 \times 0.15 \times 0.05$	$0.20 \times 0.15 \times 0.10$	$0.12 \times 0.10 \times 0.02$
Crystal system	Monoclinic	Triclinic	Monoclinic	Trigonal
Space group	C2/c	$P\bar{1}$	$P2_1/n$	$R\bar{3}c$
$a$ , Å	17.231 (3)	8.4379 (17)	9.1000 (18)	23.754 (3)
$b$ , Å	23.699 (5)	11.489 (2)	13.647 (3)	23.754 (3)
$c$ , Å	11.442 (2)	20.085 (4)	15.877 (3)	139.71 (3)
$\alpha$ , °	90	78.68 (3)	90	90
$\beta$ , °	118.93 (3)	86.99 (3)	103.10 (3)	90
$\gamma$ , °	90	75.58 (3)	90	120
$V$ , Å <sup>3</sup>	4089.7 (17)	1849.1 (7)	1920.3 (7)	68270 (26)
$Z$	4	2	2	3
$d_c$ , $\text{g cm}^{-3}$	1.301	1.431	1.515	1.330
$F(0\ 0\ 0)$	1696	832	908	28518
$\mu$ , $\text{mm}^{-1}$	1.200	1.920	2.945	2.651
$\theta_{\text{max}}$ , °	38.40	38.44	38.20	38.54



Table 1. Cont.

Compound	1-Fe	2-Zn	3-Cu	3-Ni
Index range	−20 < h < 20 −28 < k < 28 −14 < l < 4	−10 < h < 8 −12 < k < 14 −25 < l < 25	−9 < h < 10 −17 < k < 11 −19 < l < 19	−25 < h < 30 −29 < k < 25 −176 < l < 176
No. of reflections collected	24323	17994	12853	223428
No. of unique reflections ( $R_{int}$ )	4333 (0.077)	7593 (0.117)	3777 (0.080)	16597 (0.104)
No. of reflections with ( $I > 2\sigma(I)$ )	3329	4327	2436	8427
Data/restraints/parameters	4333/11/240	7593/22/387	3777/38/233	16597/31/714
$R_1; wR_2$ ( $I > 2\sigma(I)$ )	0.0568; 0.1433	0.1175; 0.2425	0.0768; 0.1762	0.0983; 0.1870
$R_1; wR_2$ (all data)	0.0764; 0.1568	0.1655; 0.2822	0.1124; 0.1980	0.1662; 0.1967
Goodness-of-fit (GOF) on $F^2$	1.171	1.046	1.057	1.084
$T_{min}; T_{max}$	0.791; 0.976	0.700; 0.900	0.550; 0.750	0.740; 0.940
$\Delta\rho_{max}; \Delta\rho_{min}, e\text{\AA}^{-3}$	0.613; −0.802	1.530; −1.319	0.800; −0.920	1.206; −0.880

### 3. Results and Discussion

#### 3.1. Spectroscopic Properties

The following changes in infrared (IR) spectra are observed ongoing, from free ligand **1** to complex **1-Fe**: the vibration band assigned to  $\nu\text{NH}$  disappears and the  $\nu\text{CH}=\text{N}$  band experiences a blueshift by  $8\text{ cm}^{-1}$ , whereas  $\nu_{as}\text{SO}_2$  and  $\nu_s\text{SO}_2$  on the contrary experience redshifts from  $1340\text{ cm}^{-1}$  and  $1164\text{ cm}^{-1}$  in **1** to  $1299$  and  $1127\text{ cm}^{-1}$  in **1-Fe**, respectively. Stretching vibrations of the imino group in 2-*N*-tosylaminobenzaldehyde azomethines are typically observed at  $1600\text{--}1630\text{ cm}^{-1}$  and they do not shift significantly upon complex formation [16,61–63]. The spectral changes observed are consistent with the deprotonation and direct involvement of the tosylamino group into the metal binding. The imino group of the azomethine moiety as well as oxygen atoms of the sulfo groups also participate in the complexation implying the formation of a chelate complex.

In the IR spectrum of the free ligand **2**, vibration bands are observed at  $3219\text{ cm}^{-1}$  (unresolved superposition of  $\nu\text{OH}$  and  $\nu\text{NH}$  signals),  $1633\text{ cm}^{-1}$  ( $\nu\text{CH}=\text{N}$ ),  $1335\text{ cm}^{-1}$  ( $\nu_{as}\text{SO}_2$ ), and  $1158\text{ cm}^{-1}$  ( $\nu_s\text{SO}_2$ ). Upon formation of the complex **2-Zn**, a new band at  $3367\text{ cm}^{-1}$  ( $\nu\text{OH}$ ) appears, whereas absorption bands  $\nu\text{CH}=\text{N}$ ,  $\nu_{as}\text{SO}_2$ , and  $\nu_s\text{SO}_2$  redshift to  $1631\text{ cm}^{-1}$ ,  $1287\text{ cm}^{-1}$ , and  $1133\text{ cm}^{-1}$ , respectively. In the  $^1\text{H}$  NMR spectrum, a proton signal of the NH group observed for the free ligand at 13.23 ppm disappears in the complex. Proton signals of the CH=N groups shift downfield from 8.36 ppm to 8.45 ppm upon complexation. Proton signals of the OH group shift similarly from 4.50 ppm and 4.68 ppm (in **2**) to 4.58 and 5.05 ppm (in **2-Zn**). This indicates that both hydroxyl groups in **2** remain free and do not participate in metal binding in **2-Zn**.

In the IR spectra of **3-Cu** and **3-Ni**, absorption bands assigned to symmetric ( $\nu_s\text{SO}_2$ ) and asymmetric ( $\nu_{as}\text{SO}_2$ ) stretching vibrations of the sulfo group redshift from  $1335\text{ cm}^{-1}$  and  $1156\text{ cm}^{-1}$  (in **3**) to  $1281\text{ cm}^{-1}$  and  $1133\text{ cm}^{-1}$  (in **3-Cu**) and to  $1297\text{ cm}^{-1}$  and  $1130\text{ cm}^{-1}$  (in **3-Ni**), respectively. The intense and broad absorption band of  $\nu\text{OH}$  groups at  $3426\text{ cm}^{-1}$  in **3** blueshifts to  $3500\text{ cm}^{-1}$  and decreases in intensity in **3-Cu** but completely disappears in **3-Ni**. A series of partly resolved bands  $\nu\text{CH}=\text{N}$  observed at  $1650\text{--}1633\text{ cm}^{-1}$  in **2** changes to well defined intense bands at  $1637\text{ cm}^{-1}$  and  $1679\text{ cm}^{-1}$  in **3-Cu** and **3-Ni**, respectively.

#### 3.2. Structure Description

##### Monomeric complexes **1-Fe** and **2-Zn**

The molecular structure of **1-Fe** is shown in Figure 2 along with the atom numbering scheme and selected bond lengths and angles. The full list of geometrical parameters for **1-Fe** is available as Supplementary Materials. The molecular structure of **1-Fe** is relatively simple and similar to a series of other related compounds characterized earlier [64–71].

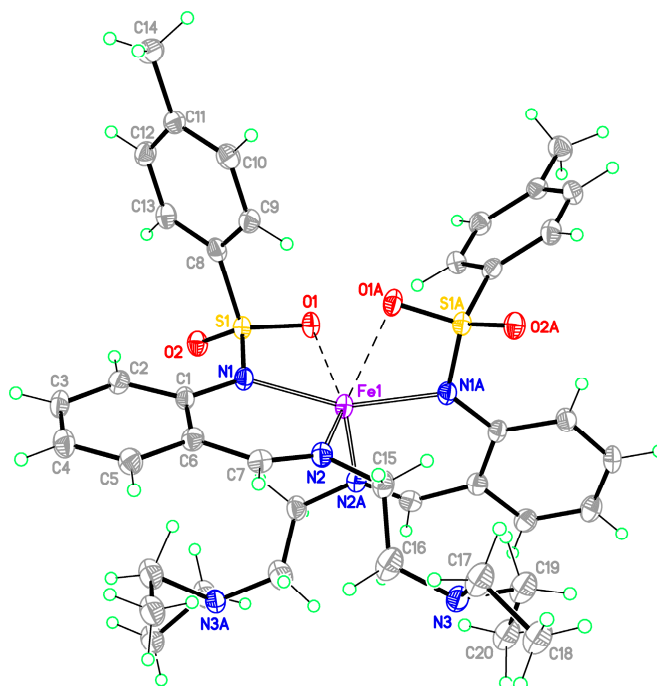


**Figure 2.** Molecular structure of **1-Fe**. Only one orientation of the disordered diethylaminoethyl substituents is presented for clarity. Displacement ellipsoids are shown at the 50% probability level. The label A denotes symmetrically equivalent atoms generated by the two-fold axis. Dashed lines indicate secondary Fe···O interactions. Selected bond lengths and angles (Å and °): Fe1–N1 2.070(2), Fe1–N2 2.102(2), Fe1···O1 2.4667(18), N1–C1 1.407(3), N2–C7 1.296(3), C1–C6 1.433(4), C6–C7 1.456(3), N1–Fe1–N2 86.41(8), N1–Fe1–N2A 107.55(8), N1–Fe1–N1A 156.79(12), N2–Fe1–N2A 107.16(11), Fe1–N1–C1 133.05(17), Fe1–N2–C7 126.95(18), N1–C1–C6 117.9(2), N2–C7–C6 128.6(2), C1–C6–C7 125.6(2).

The iron complex **1-Fe** with a metal-to-ligand ratio 1:2 is described by an idealized  $C_2$  (2) symmetry and crystallizes in the monoclinic space group  $C_2/c$ . The molecular  $C_2$  point symmetry is preserved in the crystal, i.e., the molecule occupies a special position on the two-fold axis so as only a half of it is symmetrically independent.

The iron atoms therein adopt a distorted bicapped tetrahedral “4+2” coordination environment formed by four nitrogen atoms of the tosylamino and imine groups and two weaker bonding interactions with oxygen atoms of the sulfo groups. The bond angles within the  $FeN_4$  core range from 86.41(8) to 156.79(12)° with a dihedral angle between the almost planar six-membered chelating rings (rms deviation is 0.058 Å) of 81.36(6)°. The smallest N–Fe–N angles are the intrachelate ones, whereas the largest one is that formed by the sulfonamide N atoms, i.e., N1–Fe1–N1A. Such an angle significantly increased with respect to the ideal tetrahedral value of 109.5° is determined by quite short intramolecular secondary Fe···O interactions, which are substantially shorter than those observed in related transition metal complexes. The molecular geometry observed for complex **1-Fe** is supported by four intramolecular C2–H2···O2/C2A–H2A···O2A [C···O 3.096(3), H···O 2.45 Å,  $\angle$ C–H···O 126°] and C9–H9···O1A/C9A–H9A···O1 [C···O 3.271(3), H···O 2.36 Å,  $\angle$ C–H···O 160°] hydrogen bonds.

In the crystal, molecules of **1-Fe** form stacks along the crystallographic  $c$  axis. The molecules are arranged at van der Waals distances.

The molecular structure of **2-Zn** is shown in Figure 3 along with the atom numbering scheme and selected bond lengths and angles. Despite the introduction of two hydroxy groups instead of a less coordinatively active tertiary amine, the monomeric structure similar to that in **1-Fe** is preserved. In the case of **2-Zn**, however, the molecule resides at a general position and all atoms are symmetrically independent since the structure is triclinic.



As in the case of **1-Fe**, the zinc atom in **2-Zn** adopts a distorted bicapped tetrahedral “4+2” coordination environment formed by four nitrogen atoms of the tosylamino and imine groups and two weaker bonding interactions with oxygen atoms of the sulfo groups. The bond angles within the ZnN<sub>4</sub> core range from 91.9(3) to 146.4(3)°, with a dihedral angle between the flattened six-membered chelating rings (rms deviations are 0.070 and 0.101 Å) of 78.3(2)°. It is interesting to note that the intramolecular secondary Zn···O interactions in **2-Zn** are substantially shorter and, consequently, the degree of distortion of the ZnN<sub>4</sub> tetrahedron is larger than those observed in related zinc complexes [64,67,70]. This fact can be explained by specific packing effects due to the intermolecular hydrogen bonds (Table 2, Figure 4). The molecular geometry observed for complex **2-Zn** is supported by four intramolecular C2–H2···O2 [C···O 3.062(9), H···O 2.39 Å, ∠C–H···O 128°], C19–H19···O5 [C···O 3.021(11), H···O 2.39 Å, ∠C–H···O 124°], C13–H13···O6 [C···O 3.212(9), H···O 2.27 Å, ∠C–H···O 170°] and C26–H26···O1 [C···O 3.281(9), H···O 2.36 Å, ∠C–H···O 163°] hydrogen bonds.

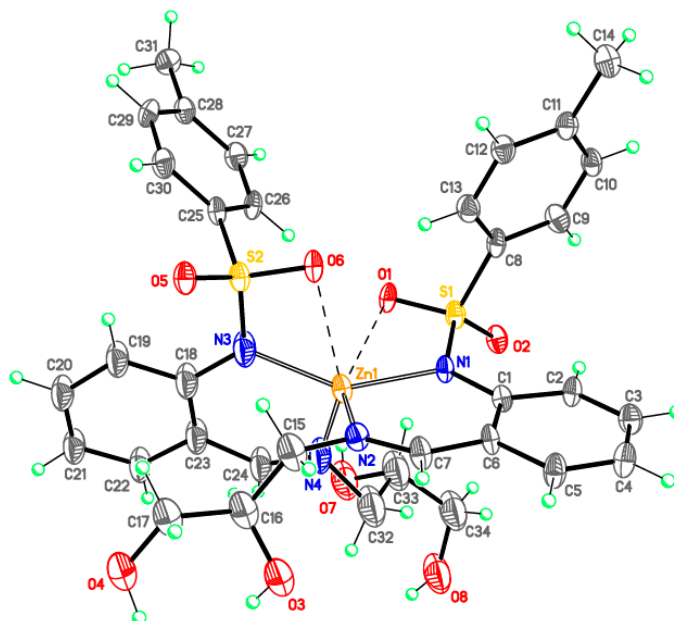


**Figure 3.** Molecular structure of **2-Zn**. The alternative orientation of the disordered 2,3-dihydroxypropyl substituent as well as the solvate dimethylformamide molecule are not shown for clarity. Displacement ellipsoids are shown at the 50% probability level. Dashed lines indicate secondary Zn...O interactions. Selected bond lengths and angles (Å and °): Zn1–N1 2.035(5), Zn1–N2 2.039(6), Zn1–N3 2.027(8), Zn1–N4 2.057(7), Zn1...O1 2.704(5), Zn1...O6 2.644(6), N1–C1 1.413(9), N2–C7 1.288(10), N2–C15 1.483(13), N3–C18 1.401(10), N4–C32 1.476(3), C6–C7 1.449(19), N1–Zn1–N2 91.8(2), N1–Zn1–N3 146.4(3), N1–Zn1–N4 104.9(3), N2–Zn1–N3 108.0(3), Zn1–N1–C1 126.7(5), Zn1–N2–C7 124.6(6), N1–C1–C6 119.8(6), N2–C7–C6 127.4(8), C1–C6–C7 127.8(7).

**Table 2.** Intermolecular hydrogen bonds in **2-Zn** [Å and °].

D–H···A	d(D–H)	d(H···A)	d(D···A)	<(DHA)
O3–H3A···O7A <sup>a</sup>	0.90	2.08	2.834(17)	140
O4–H4A···O8 <sup>a</sup>	0.90	1.95	2.84(2)	170
O4–H4A···O8A <sup>a</sup>	0.90	1.94	2.73(2)	145
O7–H7A···O3 <sup>b</sup>	0.90	1.56	2.44(2)	165
C24–H24···O8 <sup>c</sup>	0.95	2.34	3.23(2)	156
O3–H3A···O9 <sup>c</sup>	0.90	2.14	2.88(2)	139
C35–H35···O4 <sup>c</sup>	0.95	2.25	3.11(2)	151

Symmetry transformations used to generate equivalent atoms: <sup>a</sup>  $-x+2, -y+1, -z+2$ ; <sup>b</sup>  $x-1, y, z$ ; <sup>c</sup>  $-x+1, -y+1, -z+2$ ; D—proton donor; A—proton acceptor.

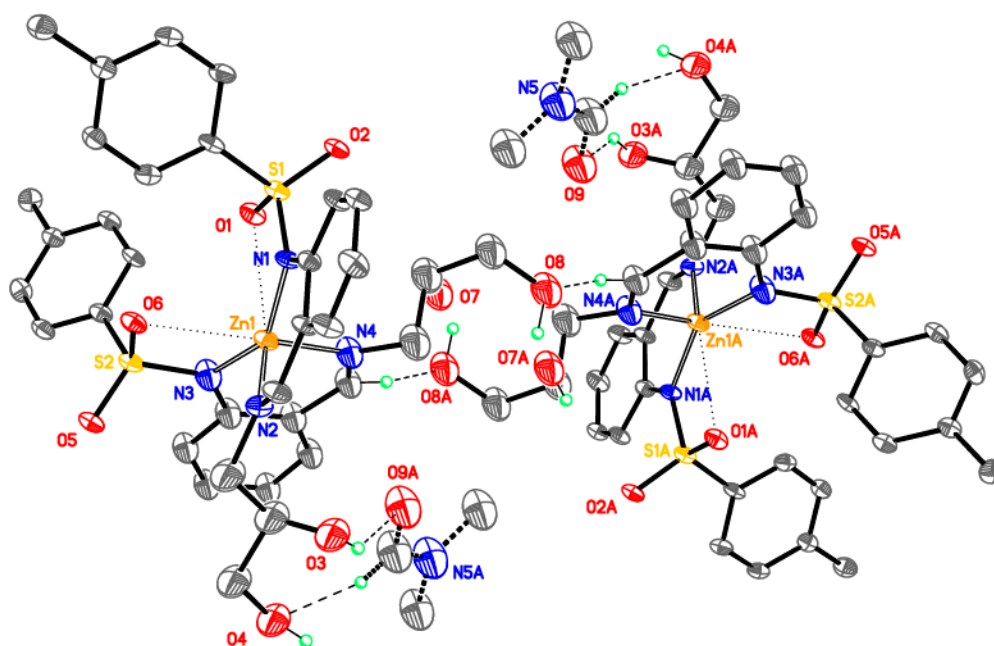


**Figure 4.** The centrosymmetric H-bonded dimers of **2-Zn**. The solvate dimethylformamide molecules with the partial occupations are depicted by thick dashed lines. Thin dashed lines indicate the intermolecular hydrogen bonds; dotted lines indicate the secondary Zn $\cdots$ O interactions.

In the crystal structure of **2-Zn**, monomeric zinc complexes and solvate dimethylformamide molecules form centrosymmetric dimers by the intermolecular C–H $\cdots$ O and O–H $\cdots$ O hydrogen bonds (Table 2, Figure 4). Additionally, the H-bonded dimers are linked by intermolecular O–H $\cdots$ O hydrogen bonds into chains propagating along the (100) direction (Figure 5).

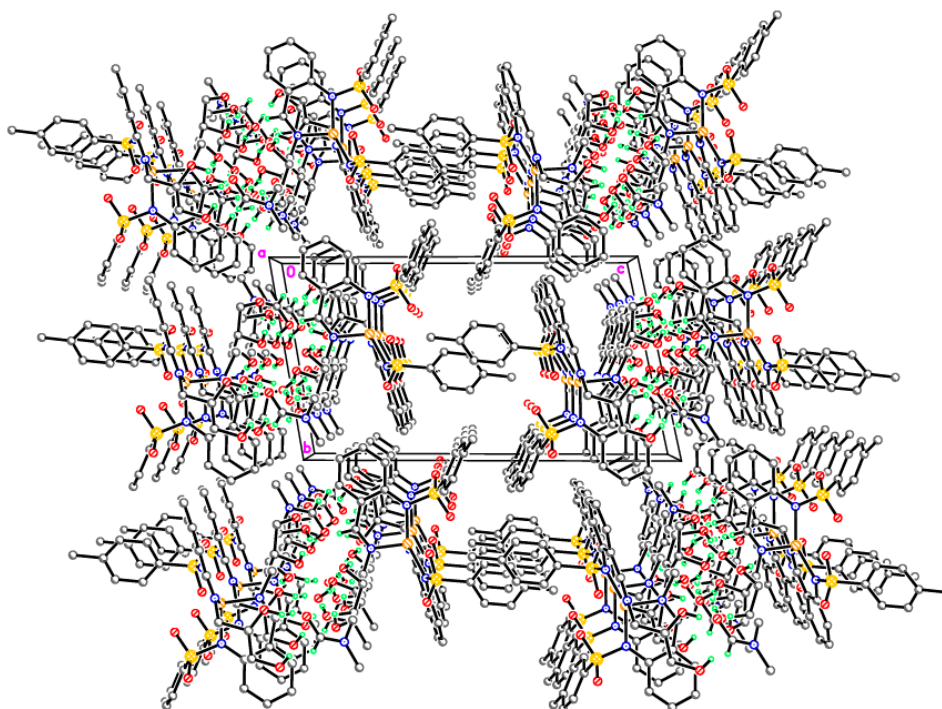


**Figure 5.** Crystal packing of **2-Zn** demonstrating the H-bonded chains of the H-bonded dimers along (100).

### Dimeric complex 3-Cu

The molecular structure of **3-Cu** is shown in Figure 6 along with the atom numbering scheme and selected bond lengths and angles. The full list of geometrical parameters for **3-Cu** is available as Supplementary Materials.

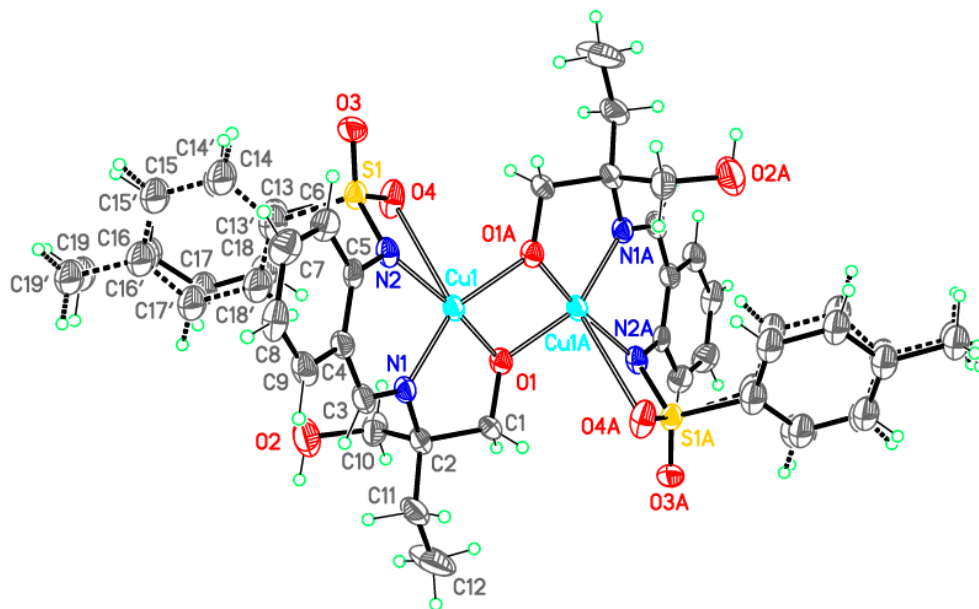


**Figure 6.** Molecular structure of **3-Cu**. Displacement ellipsoids are shown at the 50% probability level. The label A denotes symmetrically equivalent atoms generated by the inversion centre. Dashed lines indicate secondary Cu...O interactions. The alternative positions of the disordered *p*-tolyl fragments with the lesser occupations are shown by dashed lines and the respective atoms are primed. Selected bond lengths and angles (Å and °): Cu1–O1 1.918(3), Cu1–O1A 1.948(2), Cu1–N1 1.952(3), Cu1–N2 1.949(3), Cu1...O4 2.862(3), Cu1...Cu1A 2.9484(10), O1–Cu1–O1A 80.62(11), O1–Cu1–N1 84.22(12), N1–Cu1–N2 92.52(13), N2–Cu1–O1A 106.38(11), N2–Cu1–O4 56.82(10).

The ligand **3** differs from **2** in a configuration of the aliphatic diol moiety. Two OH groups in ligand **3** are located at a longer distance from each other than in **2**, which increases the conformational flexibility of the ligand, enabling it to form energetically favorable coordination bonds. As a result, a dimeric complex is formed with the nominal stoichiometry Cu<sub>2</sub>L<sub>2</sub> (L stands for the ligand **3**) with one of two hydroxy oxygen atoms within each ligand deprotonated and involved in the formation of a bridging bond between two copper atoms. The complex **3-Cu** crystallizes in the monoclinic space group P2<sub>1</sub>/*n* and occupies a special position on the inversion centre. The coordination polyhedron of the copper atoms can be described as a strongly distorted square pyramid “4+1”. Its base is formed by two nitrogen atoms (tosylamino and imine) and two hydroxy oxygen atoms. One of two oxygen atoms of the sulfo group forms a secondary bonded contact Cu...O4 as an apical vertex. *P*-tolyl fragments of the tosyl groups are disordered over two orientations related to each other by bending the (N2)–S1–C13 bond with the occupations of 0.75:0.25 (atoms belonging to the less occupied conformation have primed numbers in Figure 6).

Dimer structures also quite frequently occur among transition metal complexes with related azomethine ligands [72–75]. A close proximity of two or more metal atoms determines the magnitude of exchange interactions between paramagnetic sites and further apparent magnetic properties. In compound **3-Cu**, the Cu...Cu separation is equal to 2.9484(10) Å, which is somewhat larger than that in other reported copper complexes [74,75].

In contrast to **1-Fe** and **2-Zn**, the six-membered chelate rings in **3-Cu** are non-planar but adopt a *sofa* conformation with the deviation of the copper atom by 0.690(2) Å from the planes passed through the other atoms of the rings.

In the crystal, molecules of **3-Cu** form H-bonded layers parallel to (1 0  $\bar{1}$ ) by the intermolecular O2–H2O···O4 [O···O 3.189(4), H···O 2.28 Å,  $\angle$ O–H···O 175°] hydrogen bonds (Figure 7).

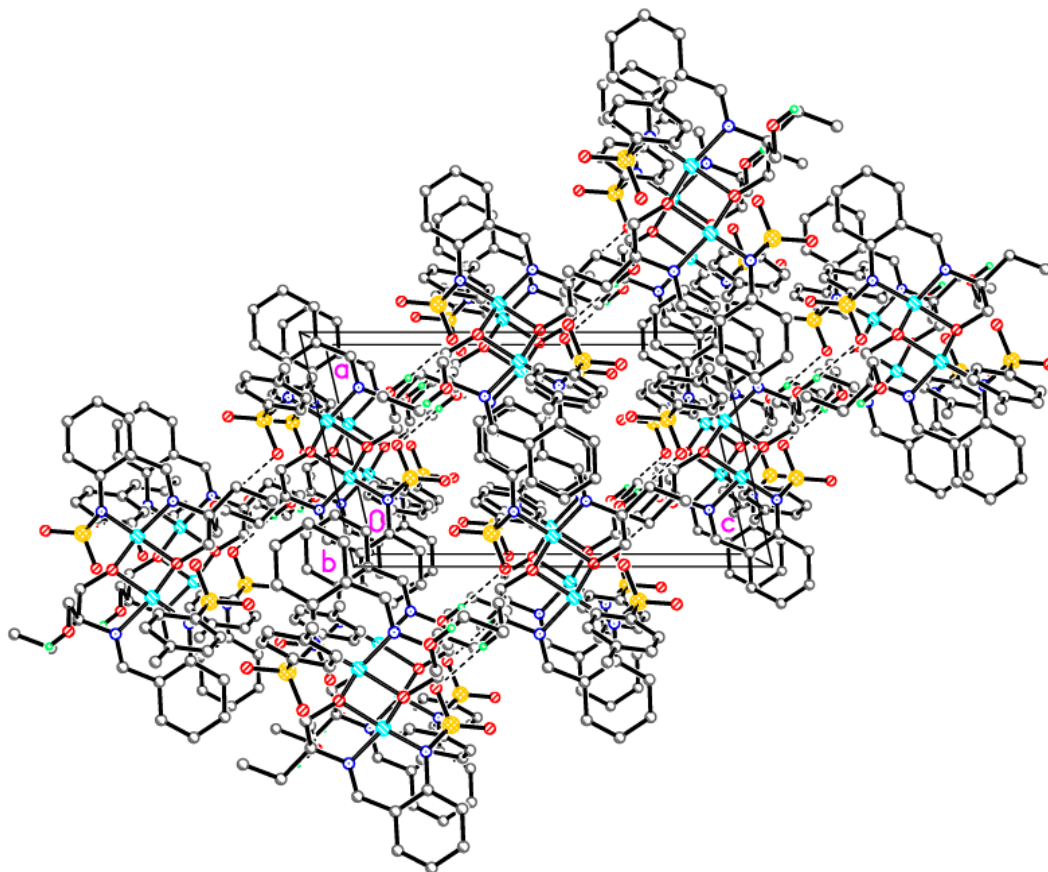


**Figure 7.** Crystal packing of **3-Cu** demonstrating the H-bonded layers parallel to (1 0  $\bar{1}$ ).

#### Supramolecular assembly of tetrameric clusters in **3-Ni**

The synthesis of **3-Ni** was performed similarly to **3-Cu** with one exception. An apparently high solubility of the product of direct interaction of free ligand **3** with a nickel salt required a pH adjustment to a more basic medium to induce the product precipitation. But the resultant structure of complex **3-Ni** revealed by single-crystal X-ray diffraction study appeared totally unexpected. The complex crystallizes in the rhombohedral space group  $R\bar{3}c$ . The overall chemical composition of **3-Ni** is rather complex and can be formulated as  $K(HNEt_3)_{0.25}[Ni_4L_3(\mu_3-O)(H_2O)_3]_3(OAc)_{1.25} \cdot 2.25AcOH$ . Cubane-like tetranuclear clusters  $Ni_4L_3(\mu_3-O)(H_2O)_3$  act as the main building blocks of the structure. Formally, they are electroneutral. Each cubane-like unit is built up of four nickel atoms, a  $\mu_3$ -oxo oxygen atom and three deprotonated hydroxy-groups of the ligands. All nickel atoms adopt a slightly distorted octahedral  $NiN_2O_4$  coordination environment (Figure 8).

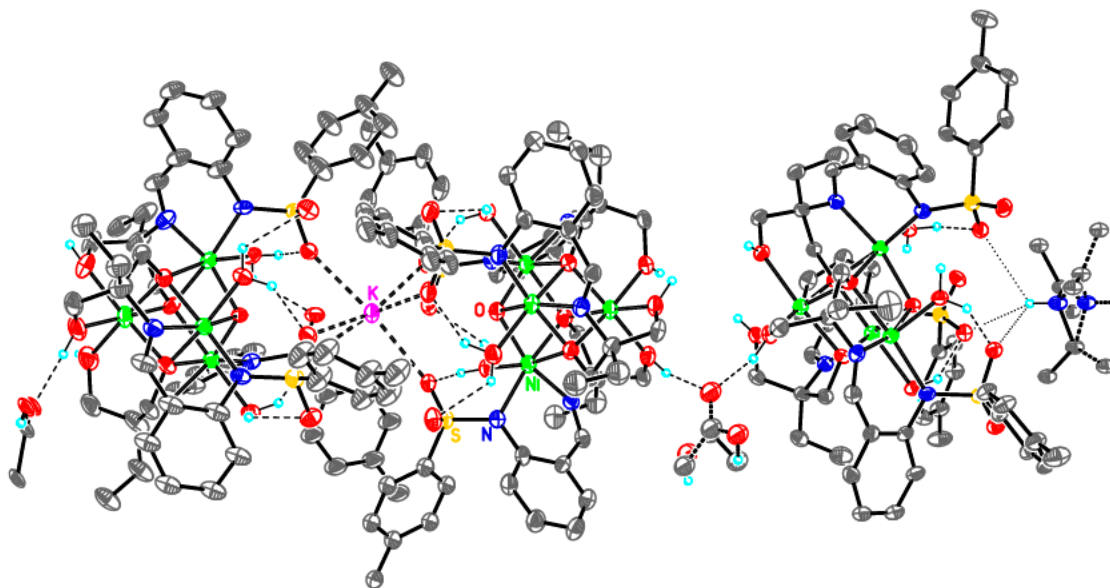


**Figure 8.** Molecular structure of **3-Ni**. Displacement ellipsoids are shown at the 50% probability level.

The Ni–O and Ni–N bond distances in **3-Ni** are 2.028(6)–2.178(5) Å and 2.005(6)–2.101(6) Å, respectively. The observed Ni–O and Ni–N bond lengths are close to those reported for a similar Ni(II) tetranuclear cubane cluster [76]. The Ni–O–Ni and O–Ni–O angles in the Ni<sub>4</sub>O<sub>4</sub> cubane cores are 95.77(18)–99.9(2)° and 79.9(2)–83.7(2)° respectively, showing a strong deviation from the idealized cubic shape. The Ni···Ni contacts in the cubane cores lie in a range 3.098(2)–3.133(2) Å.

Each Ni<sub>4</sub>L<sub>3</sub>(μ<sub>3</sub>-O)(H<sub>2</sub>O)<sub>3</sub> is located on the three-fold axis passing through one of the Ni atoms and the μ<sub>3</sub>-oxo group. Potassium cations and nitrogen atoms of the triethylammonium cations also reside at the three-fold axis. Triethylammonium cations are strongly disordered by the imposed S<sub>6</sub> ( $\bar{3}$ ) crystallographic symmetry. To achieve acceptable thermal ellipsoids, a partial occupation of the HNEt<sub>3</sub> was suggested. The net zero electrical charge of the structure is balanced by acetate anions positionally disordered with neutral acetic acid molecules.

The cubane units are linked by a cation (either K<sup>+</sup> or HNEt<sub>3</sub><sup>+</sup>) into dimers via oxygen atoms of the sulfo groups. The coordination of potassium atoms is also close to an octahedron. In turn, the dimers are joined into a chain propagating toward the crystallographic *c* axis by acetate anions via H-bonds (Table 3) involving hydroxy-groups of the ligands. The distance between centers of cubane moieties linked via K<sup>+</sup> and HNEt<sub>3</sub><sup>+</sup> are 11.086(2) Å and 13.430(2) Å, respectively. The shortest distance is realized for cubane moieties contacting via acetate anions/neutral acetic acid molecules. The respective distance between the centers of cubanes is 9.745(2) Å.

*P*-tolyl fragments of the tosyl groups forming non-polar hydrophobic exterior of the cylindrical ionically bound chains are thus responsible for the interchain packing. This packing resembles a hexagonal columnar phase (Figure 9).



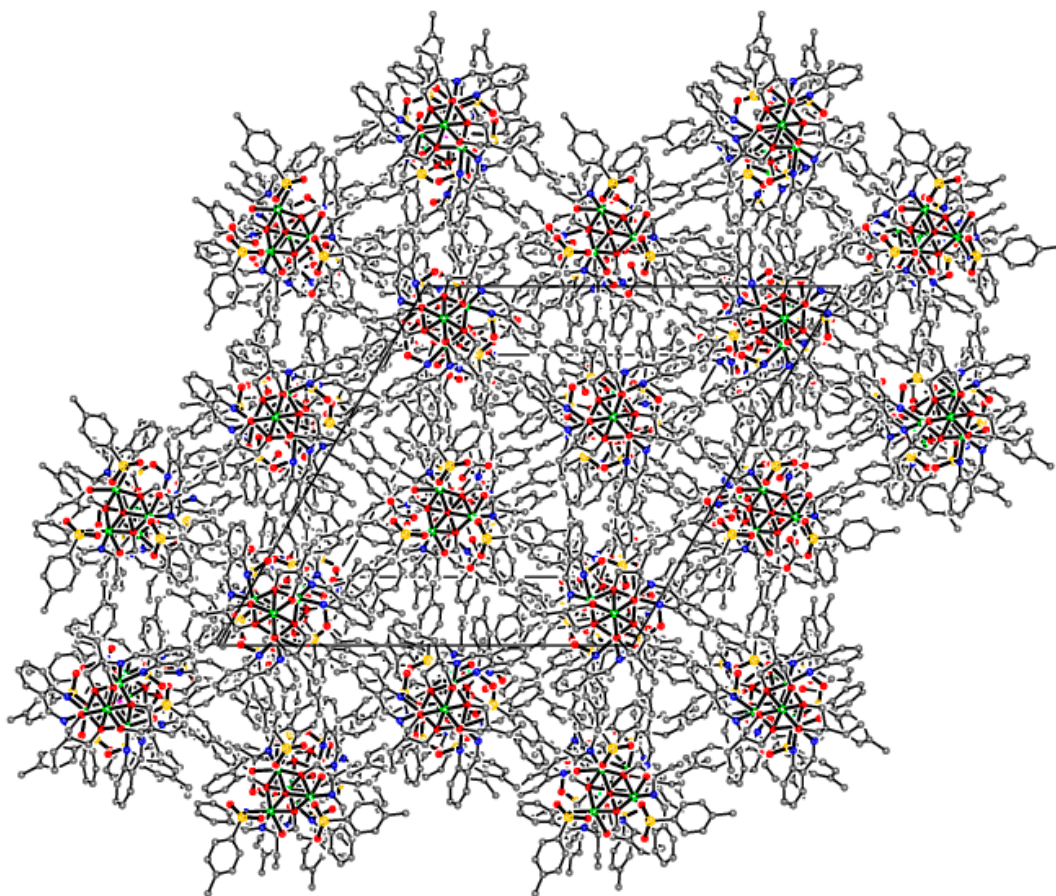


Figure 9. Crystal packing of 3-Ni along the crystallographic *c* axis.

Table 3. Hydrogen bonds for 3-Ni [Å and °].

D–H...A	d(D–H)	d(H...A)	d(D...A)	<(DHA)
O3–H3O...O19	0.92	1.72	2.616(8)	164
O6–H6A...O4	0.91	1.96	2.745(7)	145
O6–H6B...O5 <sup>a</sup>	0.91	2.22	2.916(8)	132
O9–H9O...O21	0.91	1.77	2.67(2)	169
O12–H12D...O10	0.90	1.98	2.743(7)	142
O12–H12E...O11 <sup>b</sup>	0.92	2.34	2.950(7)	124
O15–H15O...O19	0.92	1.69	2.580(8)	163
O18–H18A...O17	0.92	1.90	2.697(7)	145
O18–H18B...N6 <sup>b</sup>	0.92	2.20	3.051(7)	153

Symmetry transformations used to generate equivalent atoms: <sup>a</sup>  $-y+1, x-y+1, z$ ; <sup>b</sup>  $-x+y, -x+1, z$ .

#### 4. Conclusions

In this paper, we reported detailed crystal structures of four new transition metal complexes with 2-*N*-tosylaminobenzaldehyde azomethines bearing aliphatic amino- and alcoholic groups in the ligand's periphery. Among them, the complexes **1-Fe** and **2-Zn** are monomers with the respective metal atoms adopting distorted bicapped tetrahedral configurations with very short secondary M...O contacts involving the oxygen atoms of sulfo groups. Two complexes of copper and nickel derived from the same ligand **3**, viz. **3-Cu** and **3-Ni**, are very different structurally. Peripheral OH-groups within the ligand **3** get involved in bridging metal binding to afford a dimer with the Cu...Cu distance of 2.9484(10) Å in **3-Cu**. Meanwhile, the crystal structure of **3-Ni** reveals an unprecedented supramolecular architecture of Ni<sub>4</sub>O<sub>4</sub> cubane-type cores assembled by guest cations (K<sup>+</sup> and HNET<sub>3</sub><sup>+</sup>) and acetate anions. We attribute



this difference in the molecular structures to different coordination preferences of  $\text{Cu}^{2+}$  and  $\text{Ni}^{2+}$ . Copper ions tend to form a square planar configuration with elongated secondary interactions, whereas regular octahedral environment is strongly preferred by nickel. The abundance of water molecules in the reaction medium in the case of **3-Ni** (nickel acetate tetrahydrate was used as a Ni source) is probably responsible for the fact that water is found in the composition of the complex.

This structural variability of complexes of the title family enables fine tuning of their structure-induced practically important properties, e.g., magnetic or luminescent. The respective studies are currently in progress and their results will be a subject of future papers.

**Supplementary Materials:** Crystallographic data for all four complexes studied have been deposited with the Cambridge Crystallographic Data Center, CCDC 1578970-1578973. Copies of this information may be obtained free of charge from the Director, CCDC, 12 Union Road, Cambridge CB2 1EZ, UK (Fax: +44 1223 336033; e-mail: deposit@ccdc.cam.ac.uk or [www.ccdc.cam.ac.uk](http://www.ccdc.cam.ac.uk)). Full crystallographic tables for the four complexes studied, including atomic coordinates, bond distance and angles are also available online at [www.mdpi.com/2073-4352/7/11/325/s1](http://www.mdpi.com/2073-4352/7/11/325/s1).

**Acknowledgments:** The synthesis part of this work was financially supported by the Ministry of Education and Science of the Russian Federation (Project 4.5388.2017/8.9). Synchrotron radiation-based single-crystal X-ray diffraction measurements were performed at the unique scientific facility Kurchatov Synchrotron Radiation Source supported by the Ministry of Education and Science of the Russian Federation (project code RFMEFI61917X0007). This work was supported in part by the RUDN University Program “5-100”.

**Author Contributions:** Vladimir A. Lazarenko performed X-ray image processing, Pavel V. Dorovatovskii managed and optimized the synchrotron beamline, Yan V. Zubavichus was responsible for the diffraction measurements, Anatolii S. Burlov and Yurii V. Koshchienko synthesized the complexes for the study, Valery G. Vlasenko performed spectroscopic characterization, and Victor N. Khrustalev supervised the work and wrote the paper.

**Conflicts of Interest:** The authors declare no conflict of interests.

## References

1. Helliwell, J.R. The evolution of synchrotron radiation and the growth of its importance in crystallography. *Crystallogr. Rev.* **2013**, *18*, 32–93. [[CrossRef](#)]
2. Clegg, W. Synchrotron chemical crystallography. *J. Chem. Soc. Dalton Trans.* **2000**, *0*, 3223–3232. [[CrossRef](#)]
3. Helliwell, M. Anomalous scattering for small-molecule crystallography. *J. Synchrotron Rad.* **2000**, *7*, 139–147. [[CrossRef](#)] [[PubMed](#)]
4. Harding, M.M. Synchrotron radiation - new opportunities for chemical crystallography. *Acta Cryst.* **1995**, *B51*, 432–446. [[CrossRef](#)]
5. Coppens, P.; Cox, D.; Vlieg, E.; Robinson, I.K.; Paufler, P. *Synchrotron Radiation Crystallography*; Academic Press: London, UK, 1992; 316p, ISBN 0-12-188080-X.
6. Nowell, H.; Barnett, S.A.; Christensen, K.E.; Teat, S.J.; Allan, D.R. I19, the small-molecule single-crystal diffraction beamline at diamond light source. *J. Synchrotron Rad.* **2012**, *19*, 435–441. [[CrossRef](#)] [[PubMed](#)]
7. Allan, D.R.; Collins, S.P.; Evans, G.; Hall, D.; McAuley, K.; Owen, R.L.; Sorensen, T.; Tang, C.C.; von Delft, F.; Wagner, A.; et al. Status of the crystallography beamlines at diamond light source. *Eur. Phys. J. Plus* **2015**, *130*, 56. [[CrossRef](#)]
8. Cowieson, N.P.; Aragao, D.; Clift, M.; Ericsson, D.J.; Gee, C.; Harrop, S.J.; Mudie, N.; Panjikar, S.; Price, J.R.; Riboldi-Tunncliffe, A.; et al. MX1: A bending-magnet crystallography beamline serving both chemical and macromolecular crystallography communities at the Australian Synchrotron. *J. Synchrotron Rad.* **2015**, *22*, 187–190. [[CrossRef](#)] [[PubMed](#)]
9. Shin, J.W.; Eom, K.; Moon, D. BL2D-SMC, the supramolecular crystallography beamline at the Pohang Light Source II, Korea. *J. Synchrotron Rad.* **2016**, *23*, 369–373. [[CrossRef](#)] [[PubMed](#)]
10. Teat, S.J.; McCormick, L.J. Beamline 11.3.1. Small-Molecule Crystallography. Available online: <https://als.lbl.gov/beamlines/11-3-1> (accessed on 10 October 2017).
11. Kunz, M.; Beavers, C. Beamline 12.2.2. Diffraction Under Non-Ambient Conditions. Available online: <https://als.lbl.gov/beamlines/12-2-2> (accessed on 10 October 2017).
12. Raithby, P.R. Small-molecule chemical crystallography—from three to four dimensions: A personal perspective. *Crystallogr. Rev.* **2007**, *13*, 121–142. [[CrossRef](#)]

13. Hoshino, M.; Adachi, S.; Koshihara, S. Crystal structure analysis of molecular dynamics using synchrotron X-rays. *CrystEngComm* **2015**, *17*, 8786–8795. [[CrossRef](#)]
14. Cole, J.M. Photocrystallography. *Acta Cryst.* **2008**, *A64*, 259–271. [[CrossRef](#)] [[PubMed](#)]
15. Hatcher, L.E.; Raithby, P.R. Dynamic single-crystal diffraction studies using synchrotron radiation. *Coord. Chem. Rev.* **2014**, *277–278*, 69–79. [[CrossRef](#)]
16. Burlov, A.S.; Mal'tsev, E.I.; Vlasenko, V.G.; Garnovskii, D.A.; Dmitriev, A.V.; Lypenko, D.A.; Vannikov, A.V.; Dorovatovskii, P.V.; Lazarenko, V.A.; Zubavichus, Y.V.; et al. Synthesis, structure, photo- and electroluminescent properties of bis[(4-methyl-N-[2-[(E)-2-pyridyliminomethyl]phenyl]) benzenesulfonamide]zinc(II). *Polyhedron* **2017**, *133*, 231–237. [[CrossRef](#)]
17. Burlov, A.S.; Chesnokov, V.V.; Uraev, A.I.; Garnovskii, D.A.; Vasilchenko, I.S.; Borodkin, G.S.; Vlasenko, V.G.; Dmitriev, A.V.; Lypenko, D.A.; Maltsev, E.I.; et al. Synthesis, structure, photo- and electroluminescent properties of zinc(II) complexes with aminomethylene derivatives of 1-phenyl-3-methyl-4-formylpyrazol-5-one and 3- and 6-aminoquinolines. *Synth. Met.* **2015**, *203*, 156–163. [[CrossRef](#)]
18. Metelitsa, A.V.; Burlov, A.S.; Borodkina, I.G.; Bren, V.A.; Garnovskii, A.D.; Minkin, V.I.; Bezuglyi, S.O. Luminescent complexes with ligands containing C=N bond. *Russ. J. Coord. Chem.* **2006**, *32*, 858–868. [[CrossRef](#)]
19. Harding, M.M. The geometry of metal-ligand interactions relevant to proteins. II. Angles at the metal atom, additional weak metal-donor interactions. *Acta Cryst.* **2000**, *D56*, 857–867. [[CrossRef](#)]
20. Bertini, I.; Sigel, A. (Eds.) *Handbook on metalloproteins*; CRC Press: Boca Raton, FL, USA, 2001.
21. Andreini, C.; Bertini, I.; Cavallaro, G.; Holliday, G.L.; Thornton, J.M. Metal ions in biological catalysis: From enzyme databases to general principles. *J. Biol. Inorg. Chem.* **2008**, *13*, 1205–1218. [[CrossRef](#)] [[PubMed](#)]
22. Chohan, Z.H.; Arif, M.; Sarfraz, M. Metal-based antibacterial and antifungal amino acid derived Schiff bases: Their synthesis, characterization and in vitro biological activity. *Appl. Organomet. Chem.* **2007**, *21*, 294–302. [[CrossRef](#)]
23. Kaczmarek, M.T.; Jastrzab, R.; Holderna-Kedzia, E.; Radecka-Paryzek, W. Self-assembled synthesis, characterization and antimicrobial activity of zinc(II) salicylaldehyde complexes. *Inorg. Chim. Acta* **2009**, *362*, 3127–3133. [[CrossRef](#)]
24. Halcrow, M.A. The spin-states and spin-transitions of mononuclear iron(II) complexes of nitrogen-donor ligands. *Polyhedron* **2007**, *26*, 3523–3576. [[CrossRef](#)]
25. Harding, D.J.; Harding, P.; Phonsri, W. Spin crossover in iron(III) complexes. *Coord. Chem. Rev.* **2016**, *313*, 38–61. [[CrossRef](#)]
26. Ovcharenko, V.I.; Sagdeev, R.Z. Molecular ferromagnets. *Russ. Chem. Rev.* **1999**, *68*, 345–363. [[CrossRef](#)]
27. Pestov, A.V.; Slepukhin, P.A.; Charushin, V.N. Copper and nickel chelate complexes with polydentate N,O-ligands: Structure and magnetic properties of polynuclear complexes. *Russ. Chem. Rev.* **2015**, *84*, 310–333. [[CrossRef](#)]
28. Kogan, V.A.; Zelentsov, V.V.; Osipov, O.A.; Burlov, A.S. Dinuclear and polynuclear complexes with azomethine ligands and their magnetic properties. *Russ. Chem. Rev.* **1979**, *48*, 645–656. [[CrossRef](#)]
29. Garnovskii, A.D.; Vasilchenko, I.S.; Burlov, A.S.; Uraev, A.I.; Garnovskii, D.A. Binuclear and polynuclear complexes of Schiff bases. *Russ. J. Gen. Chem.* **2009**, *79*, 2776–2786. [[CrossRef](#)]
30. Burlov, A.S.; Nikolaevskii, S.A.; Vasilchenko, I.S.; Koshchienko, Y.V.; Uraev, A.I.; Sennikova, E.V.; Borodkin, G.S.; Garnovskii, A.D.; Minkin, V.I.; Bogomyakov, A.S.; et al. New magnetically active metal complexes of tridentate Schiff bases of phenylazosalicylaldehyde. *Russ. J. Coord. Chem.* **2009**, *35*, 486–491. [[CrossRef](#)]
31. Popov, L.D.; Tupolova, Yu.P.; Lukov, V.V.; Shcherbakov, I.N.; Burlov, A.S.; Kogan, V.A.; Ivannikova, E.V.; Levchenkov, S.I.; Lyssenko, K.A. Physico-chemical study of first row transition metal ions coordination compounds with N,N'-bis(2-tosylaminobenzylidene)-1,3-diaminopropanol. The crystal structure of bis-azomethine and its cobalt(II) complex. *Inorg. Chim. Acta* **2009**, *362*, 1673–1680. [[CrossRef](#)]
32. Emami, M.; Noshiranzadeh, N.; Bikas, R.; Gutierrez, A.; Kozakiewicz, A. Synthesis, crystal structure and magnetic studies of linear and cubane-type tetranuclear Cu(II) complexes obtained by stoichiometric control of the reagents. *Polyhedron* **2017**, *122*, 137–146. [[CrossRef](#)]
33. Kheiker, D.M.; Kovalchuk, M.V.; Shilin, Yu.N.; Shishkov, V.A.; Sulyanov, S.N.; Dorovatovskii, P.V.; Rusakov, A.A. The belok station for protein crystallography on the synchrotron radiation beam from the bending magnet in the sibir-2 storage ring. *Crystallogr. Rep.* **2007**, *52*, 358–364. [[CrossRef](#)]

34. Kabsch, W. XDS. *Acta Crystallogr.* **2010**, *D66*, 125–132. [[CrossRef](#)] [[PubMed](#)]
35. Battye, T.G.G.; Kontogiannis, L.; Johnson, O.; Powell, H.R.; Leslie, A.G.W. iMOSFLM: A new graphical interface for diffraction-image processing with MOSFLM. *Acta Crystallogr.* **2011**, *D67*, 271–281. [[CrossRef](#)] [[PubMed](#)]
36. Winn, M.D.; Ballard, C.C.; Cowtan, K.D.; Dodson, E.J.; Emsley, P.; Evans, P.R.; Keegan, R.M.; Krissinel, E.B.; Leslie, A.G.W.; McCoy, A.; et al. Overview of the CCP4 suite and current developments. *Acta Crystallogr.* **2011**, *D67*, 235–242.
37. Sauter, N.K.; Hattne, J.; Grosse-Kunstleve, R.W.; Echols, N. New Python-based methods for data processing. *Acta Crystallogr.* **2013**, *D69*, 1274–1282. [[CrossRef](#)] [[PubMed](#)]
38. Evans, P. Scaling and assessment of data quality. *Acta Crystallogr.* **2006**, *D62*, 72–82. [[CrossRef](#)] [[PubMed](#)]
39. Dolomanov, O.V.; Bourhis, L.J.; Gildea, R.J.; Howard, J.A.K.; Puschmann, H. OLEX2: A complete structure solution, refinement and analysis program. *J. Appl. Crystallogr.* **2009**, *42*, 339–341. [[CrossRef](#)]
40. Sheldrick, G.M. A short history of SHELX. *Acta Crystallogr.* **2008**, *A64*, 112–122. [[CrossRef](#)] [[PubMed](#)]
41. Sheldrick, G.M. Crystal structure refinement with SHELXL. *Acta Crystallogr.* **2015**, *C71*, 3–8.
42. Sheldrick, G.M. SHELXT - Integrated space-group and crystal-structure determination. *Acta Crystallogr.* **2015**, *A71*, 3–8. [[CrossRef](#)] [[PubMed](#)]
43. Safonova, T.N.; Mordkovich, N.N.; Veiko, V.P.; Okorokova, N.A.; Manuvera, V.A.; Dorovatovskii, P.V.; Popov, V.O.; Polyakov, K.M. Concerted action of two subunits of the functional dimer of *Shewanella oneidensis* MR-1 uridine phosphorylase derived from a comparison of the C212S mutant and the wild-type enzyme. *Acta Crystallogr.* **2016**, *D72*, 203–210.
44. Osipov, E.M.; Polyakov, K.M.; Tikhonova, T.V.; Kittl, R.; Dorovatovskii, P.V.; Shleev, S.V.; Popov, V.O.; Ludwig, R. Incorporation of copper ions into crystals of T2 copper-depleted laccase from *Botrytis aclada*. *Acta Crystallogr.* **2016**, *F71*, 1465–1469.
45. Glazunova, O.A.; Polyakov, K.M.; Fedorova, T.V.; Dorovatovskii, P.V.; Koroleva, O.V. Elucidation of the crystal structure of *Corioliopsis caperata* laccase: Restoration of the structure and activity of the native enzyme from the T2-depleted form by copper ions. *Acta Crystallogr.* **2015**, *D71*, 854–861.
46. Osipov, E.; Polyakov, K.; Kittl, R.; Shleev, S.; Dorovatovskii, P.; Tikhonova, T.; Hann, S.; Ludwig, R.; Popov, V. Effect of the L499M mutation of the ascomycetous *Botrytis aclada* laccase on redox potential and catalytic properties. *Acta Crystallogr.* **2013**, *D70*, 2913–2923.
47. Mitkevich, V.A.; Schulga, A.A.; Trofimov, A.A.; Dorovatovskii, P.V.; Goncharuk, D.A.; Tkach, E.N.; Makarov, A.A.; Polyakov, K.M. Structure and functional studies of the ribonuclease binase Glu43Ala/Phe81Ala mutant. *Crystallogr.* **2013**, *D69*, 991–996. [[CrossRef](#)] [[PubMed](#)]
48. Tursina, A.I.; Nesterenko, S.N.; Chernyshev, V.V.; Sulyanov, S.N.; Dorovatovskii, P.V.; Britz, D.; Strydom, A.M. Synthesis, structure and physical characterization of the structural transitions in CePd<sub>3</sub>Sn and LaPd<sub>3</sub>Sn polymorphs. *J. Alloys Comp.* **2016**, *688*, 1162–1171. [[CrossRef](#)]
49. Petrov, A.A.; Sokolova, I.P.; Belich, N.A.; Peters, G.S.; Dorovatovskii, P.V.; Zubavichus, Y.V.; Khrustalev, V.N.; Petrov, A.V.; Grätzel, M.; Goodilin, E.A.; et al. Crystal structure of DMF-intermediate phases uncovers the link between CH<sub>3</sub>NH<sub>3</sub>PbI<sub>3</sub> morphology and precursor's stoichiometry. *J. Phys. Chem. C* **2017**, *21*, 20739–20743. [[CrossRef](#)]
50. Pozhidaev, E.P.; Torgova, S.I.; Barbashov, V.A.; Minchenko, M.V.; Sulyanov, S.N.; Dorovatovskii, P.V.; Ostrovskii, B.I.; Strigazzi, A. Ferroelectric C\* phase induced in a nematic liquid crystal matrix by a chiral non-mesogenic dopant. *Appl. Phys. Lett.* **2015**, *106*, 062904. [[CrossRef](#)]
51. Trofimchuk, E.S.; Efimov, A.V.; Grokhovskaya, T.E.; Nikonorova, N.I.; Moskvina, M.A.; Sedush, N.G.; Dorovatovskii, P.V.; Ivanova, O.A.; Rukhlya, E.G.; Volynskii, A.L.; et al. Cold crystallization of glassy polylactide during solvent crazing. *ACS Appl. Mater. Inter.* **2017**, *9*, 34325–34336. [[CrossRef](#)] [[PubMed](#)]
52. Bilyachenko, A.N.; Kulakova, A.N.; Levitsky, M.M.; Petrov, A.A.; Korlyukov, A.A.; Shul'pina, L.S.; Khrustalev, V.N.; Dorovatovskii, P.V.; Vologzhanina, A.V.; Tsareva, U.S.; et al. Unusual tri-, hexa-, and nonanuclear Cu(II) cage methylsilsesquioxanes: Synthesis, structures, and catalytic activity in oxidations with peroxides. *Inorg. Chem.* **2017**, *56*, 4093–4103. [[CrossRef](#)] [[PubMed](#)]
53. Yalymov, A.I.; Bilyachenko, A.N.; Levitsky, M.M.; Korlyukov, A.A.; Khrustalev, V.N.; Shul'pina, L.S.; Dorovatovskii, P.V.; Es'kova, M.A.; Lamaty, F.; Bantreil, X.; et al. High catalytic activity of heterometallic (Fe<sub>6</sub>Na<sub>7</sub> and Fe<sub>6</sub>Na<sub>6</sub>) cage silsesquioxanes in oxidations with peroxides. *Catalysts* **2017**, *7*, 101. [[CrossRef](#)]

54. Bilyachenko, A.N.; Korlyukov, A.A.; Vologzhanina, A.V.; Khrustalev, V.N.; Kulakova, A.N.; Long, J.; Larionova, J.; Guari, Y.; Dronova, M.; Tsareva, U.; et al. Tuning linkage isomerism and magnetic properties of bi- and tri-metallic cage silsesquioxanes by cation and solvent effects. *Dalt. Trans.* **2017**, *46*, 12935–12949. [[CrossRef](#)] [[PubMed](#)]
55. Krasnov, K.A.; Dorovatovskii, P.V.; Zubavichus, Y.V.; Timofeeva, T.V.; Khrustalev, V.N. Hydride transfer reactions of 5-(2-alkohybenzylidene) barbituric acids: Synthesis of 2,4,6-trioxoperhydropyrimidine-5-spiro-3'-chromanes. *Tetrahedron* **2017**, *73*, 542–549. [[CrossRef](#)]
56. Zubkov, F.I.; Kvyatkovskaya, E.A.; Nikitina, E.V.; Amoyaw, P.; Kouznetsov, V.; Lazarenko, V.; Khrustalev, V.N. Comment on “An unexpected formation of the novel 7-oxa-2-azabicyclo[2.2.1]hept-5-ene skeleton during the reaction of furfurylamine with maleimides and their bioprospection using a zebrafish embryo model” by C. E. Puerto Galvis and V. V. Kouznetsov, *Org. Biomol. Chem.*, 2013, 11, 407. *Org. Biomol. Chem.* **2017**, *15*, 6447–6450. [[PubMed](#)]
57. Astakhov, A.V.; Khazipov, O.V.; Chernenko, A.Y.; Pasyukov, D.V.; Kashin, A.; Gordeev, E.G.; Khrustalev, V.N.; Chernyshev, V.M.; Ananikov, V.P. A new mode of operation of Pd-NHC systems studied in a catalytic mizoroki–heck reaction. *Organometallics* **2017**, *36*, 1981–1992. [[CrossRef](#)]
58. Zubkevich, S.V.; Gagieva, S.C.; Tuskaev, V.A.; Dorovatovskii, P.V.; Khrustalev, V.N.; Sizov, A.I.; Bulychev, B.M. Synthesis and reactivity in ethylene oligomerization by heteroscorpionate dibromonickel (II) complexes. *Inorg. Chim. Acta* **2017**, *458*, 58–67. [[CrossRef](#)]
59. Vologzhanina, A.V.; Avdeeva, V.V.; Buzin, M.I.; Dmitrienko, A.O.; Dorovatovskii, P.V.; Malinina, E.A.; Kuznetsov, N.T.; Voronova, E.D.; Zubavichus, Y.V. Solid-State reactions of eicosaborate [B<sub>20</sub>H<sub>18</sub>]<sup>2-</sup> salts and complexes. *Chem. Eur. J.* **2017**, in press. [[CrossRef](#)] [[PubMed](#)]
60. Chernova, N.I.; Ryabokobylko, Y.S.; Brudz, V.G.; Bolotin, B.M. 2-Tosylaminobenzaldehyde and its substitutes. *Zh. Org. Khim.* **1971**, *7*, 1680–1687.
61. Sousa-Pedrares, A.; Viqueira, J.A.; Antelo, J.; Labisbal, E.; Romero, J.; Sousa, A.; Nascimento, O.R.; García-Vázquez, J.A. Synthesis and characterization of homoleptic and heteroleptic cobalt, nickel, copper, zinc and cadmium compounds with the 2-(Tosylamino)-N-[2-(tosylamino)benzylidene]aniline ligand. *Eur. J. Inorg. Chem.* **2011**, *2011*, 2273–2287. [[CrossRef](#)]
62. Labisbal, E.; Rodríguez, L.; Sousa-Pedrares, A.; Alonso, M.; Vizoso, A.; Romero, J.; García-Vázquez, J.A.; Sousa, A. Synthesis, characterisation and X-ray structures of diorganotin(IV) and iron(III) complexes of dianionic terdentate Schiff base ligands. *J. Organomet. Chem.* **2006**, *691*, 1321–1332. [[CrossRef](#)]
63. Burlov, A.S.; Vlasenko, V.G.; Makarova, N.I.; Lyssenko, K.A.; Chesnokov, V.V.; Borodkin, G.S.; Vasilchenko, I.S.; Uraev, A.I.; Garnovskii, D.A.; Metelitsa, A.V. Chemical and electrochemical synthesis, molecular structures, DFT calculations and optical properties of metal-chelates of 8-(2-tosylaminobenzylideneimino)quinolone. *Polyhedron* **2016**, *107*, 153–162. [[CrossRef](#)]
64. Martin, D.; Rouffet, M.; Cohen, S.M. Illuminating metal-ion sensors: Benzimidazolesulfonamide metal complexes. *Inorg. Chem.* **2010**, *49*, 10226–10228. [[CrossRef](#)] [[PubMed](#)]
65. Cabaleiro, S.; Perez-Lourido, P.; Castro, J.; Romero, J.; Garcia-Vazquez, J.A.; Sousa, A. Copper(II) [(4-methylphenyl)sulfonyl]-1H-imino-(2-phenyl-2-oxazoline) complexes. *Transition Met. Chem.* **2001**, *26*, 709–716. [[CrossRef](#)]
66. Dorokhov, A.V.; Chernyshov, D.Yu.; Burlov, A.S.; Garnovskii, A.D.; Ivanova, I.S.; Pyatova, E.N.; Tsivadze, A.Yu.; Aslanov, L.A.; Chernyshev, V.V. Synchrotron powder diffraction in a systematic study of 4'-[2-(tosylamino)benzylideneamino]-2,3-benzo-15-crown-5 complexes. *Acta Crystallogr.* **2007**, *B63*, 402–410. [[CrossRef](#)] [[PubMed](#)]
67. Minacheva, L.K.; Ivanova, I.S.; Dorokhov, A.V.; Burlov, A.S.; Garnovsky, A.D.; Sergienko, V.S.; Tsivadze, A.Y. Zn complex with N-(4'-Benzo-15-crown-5)-2-(amino-N-tosyl)-phenylaldimine: Synthesis, crystal structure, and vibration spectrum. *Russ. J. Coord. Chem.* **2006**, *32*, 166–172. [[CrossRef](#)]
68. Garcia-Vazquez, J.A.; Romero, J.; Duran, M.L.; Sousa, A.; Garnovskii, A.D.; Burlov, A.S.; Garnovskii, D.A. Electrochemical synthesis of metal (II) complexes of Schiff base 2-tosylamino (2'-pyridyl)aniline: The crystal structure of bis-[2-tosylamino(2'-pyridyl)anilinato]cobalt(II). *Polyhedron* **1998**, *17*, 1547–1552. [[CrossRef](#)]
69. Castro, J.; Cabaleiro, S.; Perez-Lourido, P.; Romero, J.; Garcia-Vazquez, J.A.; Sousa, A. Electrochemical synthesis, X-ray diffraction and spectroscopic characterisation of Co(II) compounds with [(4-methylphenyl)sulfonyl]-1H-imino-2-phenyl-2-oxazolines. *Polyhedron* **2001**, *20*, 2329–2337. [[CrossRef](#)]

70. Castro, J.; Cabaleiro, S.; Perez-Lourido, P.; Romero, J.; Garcia-Vazquez, J.A.; Sousa, A. Electrochemical synthesis and characterization of Zinc(II) complexes with [(4-methylphenyl)sulfonyl]-1h-amido-2-phenyl-2-oxazolines. *Z. Anorg. Allg. Chem.* **2002**, *628*, 1210–1217. [[CrossRef](#)]
71. Li, J.; Tian, D.; Song, H.; Wang, C.; Zhu, X.; Cui, C.; Cheng, J.P. Synthesis, structures, and reactivity of nickel complexes incorporating sulfonamido-imine ligands. *Organometallics* **2008**, *27*, 1605–1611. [[CrossRef](#)]
72. Garnovskii, A.D.; Burlov, A.S.; Garnovskii, D.A.; Vasilchenko, I.S.; Antsichkina, A.S.; Sadikov, G.G.; Sousa, A.; Garcia-Vazquez, J.A.; Romero, J.; Duran, M.L.; et al. Synthesis of cobalt(II), nickel(II) and copper(II) complexes with 2-(2-hydroxyphenyliminomethyl)-1-(4-methyl-phenylsulfonamido)benzene and crystal structures of {bis(methanol)[2-(2'-N-tosylaminophenyl)iminomethyl]phenolato}nickel(II) and {bis(2,2'-bipyridine)[2-(2'-N-tosylaminophenyl)iminomethyl]phenolato}copper(II). *Polyhedron* **1999**, *18*, 863–869.
73. Antsyshkina, A.S.; Sadikov, G.G.; Burlov, A.S.; Vasil'chenko, I.S.; Garnovskii, A.D.; Sergienko, V.S. Synthesis and crystal and molecular structure of the solvate (1:4) of Bis {(methanol)(2-[2'-(N-tosylaminophenyl)iminomethyl] phenolato) cobalt (II)} with Methanol. *Russ. J. Inorg. Chem.* **2000**, *45*, 1666–1670.
74. Uraev, A.I.; Vasilchenko, I.S.; Ikorskii, V.N.; Shestakova, T.A.; Burlov, A.S.; Lyssenko, K.A.; Vlasenko, V.G.; Kuz'menko, T.A.; Divaeva, L.N.; Pirog, I.V.; et al. Copper(II) dimers with ferromagnetic intra- and intermolecular exchange interactions. *Mendeleev Commun.* **2005**, *15*, 133–135. [[CrossRef](#)]
75. Sanmartin, J.; Novio, F.; Garcia-Deibe, A.M.; Fondo, M.; Ocampo, N.; Bermejo, M.R. Dimeric complexes of a tridentate schiff base ligand – crystal structure of a cu(II) complex with uncommon  $\mu_2$ -N<sub>sulfonamido</sub> bridges and ferromagnetic behaviour. *Eur. J. Inorg. Chem.* **2008**, *2008*, 1719–1726. [[CrossRef](#)]
76. Jana, M.S.; Priego, J.L.; Jimenez-Aparicio, R.; Mondal, T.K. Novel tetranuclear Ni(II) schiff base complex containing Ni<sub>4</sub>O<sub>4</sub> cubane core: Synthesis, X-ray structure, spectra and magnetic properties. *Spectrochim. Acta A* **2014**, *133*, 714–719. [[CrossRef](#)] [[PubMed](#)]



© 2017 by the authors. Licensee MDPI, Basel, Switzerland. This article is an open access article distributed under the terms and conditions of the Creative Commons Attribution (CC BY) license (<http://creativecommons.org/licenses/by/4.0/>).